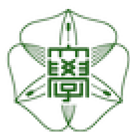

Title	Precise Structural Control of GaN Porous Nanostructures Utilizing Anisotropic Electrochemical and Chemical Etching for the Optical and Photoelectrochemical Applications
Author(s)	Kumazaki, Yusuke; Matsumoto, Satoru; Sato, Taketomo
Citation	Journal of The Electrochemical Society, 164(7), H477-H483 https://doi.org/10.1149/2.0771707jes
Issue Date	2017-05-12
Doc URL	http://hdl.handle.net/2115/66290
Rights(URL)	http://creativecommons.org/licenses/by/4.0/
Type	article
File Information	J. Electrochem. Soc.-2017-Kumazaki-H477-83.pdf (本文)

Instructions for use

Hokkaido University Collection of Scholarly and Academic Papers : HUSCAP

Journal of The Electrochemical Society, **164** (7) H477-H483 (2017)

Precise Structural Control of GaN Porous Nanostructures Utilizing Anisotropic Electrochemical and Chemical Etching for the Optical and Photoelectrochemical Applications

Yusuke Kumazaki,[z] Satoru Matsumoto, and Taketomo Sato[*]

Research Center for Integrated Quantum Electronics and Graduate School of Information Science and Technology, Hokkaido University, Sapporo 060-8628, Japan

A low-damaged wet process utilizing electrochemical (EC) etching and subsequent chemical etching has been developed for the fabrication of GaN porous structures. Superior controllability in depth and diameter could be obtained by achieving anisotropic nature of the vertical direction to the substrate by EC etching and horizontal direction by tetramethylammonium hydroxide (TMAH) etching, respectively. The optical and photoelectrochemical properties of GaN porous structures were very sensitive to the structural properties. Photoreflectance measurement revealed that porous sample had an effective refractive index that could be controlled by TMAH etching time. In photoelectrochemical measurement, the incident-photon-to-current conversion efficiency (IPCE) was dramatically enhanced to as high as 91% by the formation of porous structures. A series of experimental results were consistently explained by the change of thickness of pore wall and width of space charge region.
© The Author(s) 2017. Published by ECS. This is an open access article distributed under the terms of the Creative Commons Attribution 4.0 License (CC BY, http://creativecommons.org/licenses/by/4.0/), which permits unrestricted reuse of the work in any medium, provided the original work is properly cited. [DOI: 10.1149/2.0771707jes] All rights reserved.

Manuscript submitted January 26, 2017; revised manuscript received April 14, 2017. Published May 12, 2017. This was Paper 1253 presented at the Honolulu, Hawaii, Meeting of the Society, October 2–7, 2016.

Gallium nitride (GaN) and its alloys are getting much attention as building block materials for electrochemical (EC) energy conversion systems such as chemical sensors, water splitting, and artificial photosynthesis because of their attractive features including superior chemical stability, direct transition, and widely tunable bandgap by alloying.[1–4] Among the various techniques for improving their conversion efficiency, porosification utilizing EC reactions is one of the most powerful because a high-density array of pores exhibits high specific surface area, low reflectance, and high absorptance properties.[5,6] In addition, this technique is performed at room temperature and does not require any complicated process such as lithography, indicating lower damage and higher productivity than other nanostructure fabrication techniques such as reactive ion etching and selective-area growth.[7–10]

Many reports involving porosification use photo-assisted EC etching utilizing charge carriers generated by band-edge absorption.[11–14] Our group has also succeeded in forming GaN porous nanostructures by photo-assisted EC etching and found the energy-conversion efficiency to be enhanced compared with the planar substrate.[15] However, the pore depth could not be controlled linearly by etching time, resulting in difficulty with forming pores deeper than a micro-meter. This was because charge carriers, most of which were generated near the top surface, were expended preferentially in the lateral etching of pore walls that appeared on the top surface. Such insufficient anisotropic nature makes it difficult to improve structural controllability and form pores deeper than a micro-meter.

In this study, we aimed to develop anisotropic EC etching by utilizing charge carriers generated by the avalanche effect as a porosification process. We also investigated a combination of EC etching and subsequent wet chemical etching to further improve the structural controllability. Optical characterization such as photoluminescence (PL), photoreflectance, and photoelectrochemical measurements revealed the importance of precise structural controlling of porous structures on application to the energy conversion systems.

Methods

In this study, we used an n-type GaN (0001) freestanding wafer with the threading dislocation density (TDD) of 3.7×10^6 cm^{-2} which is commercially available from SCIOCS COMPANY LIMITED. Carrier concentration N_D and thickness were 1.1×10^{18} cm^{-3} and 400 μm, respectively. Ti (20 nm)/Au (50 nm) bilayer ohmic electrode was formed on the back side of the substrate by an electron-beam evaporation method. For the porosification, EC etching was performed using a three-electrode type cell consisting of an n-type GaN working electrode, a Pt counter electrode, and a Ag/AgCl reference electrode in mixture of 1 mol/L H_2SO_4 and 1 mol/L H_3PO_4 (pH = 1.7) as an electrolyte. We applied a constant voltage V_{EC} precisely controlled by a potentiostat with a Princeton Applied Research VersaSTAT 4 to cause EC reactions.

We have reported that the direction of pore growth was changed in accordance with V_{EC} applied under the dark condition, whose formation has been discussed in detail previously.[16] In this study, we set the V_{EC} at 10 V to obtain the straight pores oriented perpendicular to the top surface, where the pore branching was significantly suppressed. The structural properties of the porous samples formed by the anisotropic EC etching were compared with those formed by the photo-assisted EC etching as a function of the etching time t_{EC}. After the porosification, wet chemical etching was carried out in 25% tetramethylammonium hydroxide (TMAH) at 90°C. The TMAH solution was not stirred during the chemical etching. Since TMAH is known as an anisotropic etchant of GaN with a very slow etching rate, it is favorable for precise structural control.[17,18] The structural properties of the GaN porous structures were evaluated by scanning electron microscopy (SEM) with a Hitachi SU-8010 system. PL measurements were carried out using an optical multichannel analyzer system (Acton Research Corporation) and a He-Cd laser with an intensity of 0.1 mW/cm^2 at a wavelength λ of 325 nm. Specular reflectance properties were investigated using a UV-VIS spectrophotometer with a Shimadzu UV-1700. In view of possible use in EC energy conversion systems, photoelectrochemical characteristics were investigated in 0.1 mol/L phosphate buffer solution (PBS, pH = 7.4) under monochromatic light irradiated from a Xe lamp through an optical band-path filter with a FWHM of 10 nm.

Results and Discussion

Formation of GaN porous structures by EC etching.—The two kinds of EC etching were conducted for the porosification of GaN surface and their structural controllability was compared. Figure 1a shows a cross-sectional SEM image of the GaN porous structures formed by photo-assisted EC etching conducted under light with voltage V_{EC} of 1.0 V and etching time t_{EC} of 10 min. A high-density array of [000−1]-oriented pores were formed on the surface, but pore depth and diameter were inhomogeneous. These features were strongly correlated with the method of supplying positive holes causing EC reactions. Under the light with photon energy above bandgap, concentration of positive holes in the valence band is significantly

*Electrochemical Society Member.
[z]E-mail: kumazaki@rciqe.hokudai.ac.jp

Downloaded on 2017-06-27 to IP 133.87.166.83 address. Redistribution subject to ECS terms of use (see ecsdl.org/site/terms_use) unless CC License in place (see abstract).

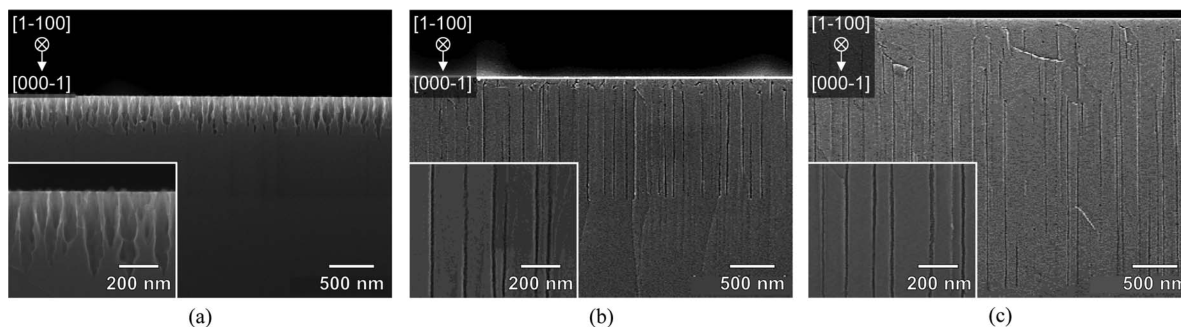

Figure 1. Cross-sectional SEM images of GaN porous nanostructures formed under various electrochemical conditions: (a) under light, $V_{EC} = 1.0$ V, $t_{EC} = 10$ min, (b) in dark, $V_{EC} = 10$ V, $t_{EC} = 20$ min, and (c) in dark, $V_{EC} = 10$ V, $t_{EC} = 40$ min.

increased by band-edge absorption since hole is a minority carrier in n-type material. Then, positive holes are transferred to the pore tips at which electric field lines concentrated, leading to etching in the vertical direction. However, the number of positive holes transferred to pore tips decreases with increase of pore depth because of the short light penetration depth (< 100 nm[19]) in GaN, leading to etching in the lateral direction on the top surface. This is a brief description of why the photo-assisted EC etching shows insufficient anisotropic nature. Details are described in our previous work.[15]

Figures 1b and 1c show cross-sectional SEM images of the GaN porous structures formed in the dark with V_{EC} of 10 V and t_{EC} of 20 min and 40 min, respectively. Both samples had two kinds of porous regions consisting of randomly oriented pores near the top surface and vertically oriented pores in the [000−1] direction underneath. Pore depth D_p increased from 1360 nm to 3000 nm with t_{EC} increase, whereas pore diameter W_p remained unchanged. This result clearly demonstrates that EC etching in the dark proceeds anisotropically in the [000−1] direction and not preferentially in other directions.

Many previous studies on porous GaN have reported that the pore density and etching profile strongly correlated with dislocations of GaN crystal.[20,21] In these reports, hetero-epitaxial GaN films grown on sapphire substrates were used, where the TDD of GaN crystal was typically 10^9 to 10^{10} cm^{-2}. In the case of such high TDD, the positive holes supplied to EC reactions would be strongly affected by the dislocations, which acted as recombination centers. In this study, however, TDD of the freestanding GaN wafer was 3.7×10^6 cm^{-2}, which is four orders of magnitude less than the pore density of 2.0×10^{10} cm^{-2}.

We tried to describe the mechanism of anisotropic pore formation in EC etching in the dark by referring to the "Beale model", which was first applied for porous Si.[22,23] According to this model, the pores grow up along two notable phenomena: (1) structural inhomogeneities induce localization of charge carrier flow by electric field enhancement in the space charge region (SCR), and (2) fully depleted pore wall (semiconductor between pores) is highly resistive, which prevents charge carrier flow and further EC reactions. On the basis of these pictures, anisotropic pore formation observed here is schematically described in Fig. 2. At the initial stage, trenches are formed by EC etching at locations that are chemically unstable and/or where the electric field is concentrated (Fig. 2a). Although it remains unclear where initial etching occurs, it seems Ga-vacancies V_{Ga} (or related complexes) are possible initiation sites. Evidently, PL measurements revealed that yellow luminescence were diminished by EC etching (discussed in detail in section Optical and photoelectrochemical properties of GaN porous structures). Once the trenches are formed, a high electric field is induced on trenches. If the enhanced electric field reaches the breakdown limit, charge carriers are generated by avalanche effect. In this way, the randomly oriented pores are grown from trenches (Fig. 2b). When the neighboring pores approach one another, the electric field around the side walls of the pores becomes small due to the merging of SCRs (Fig. 2c).[24] In such situation, charge carriers can be generated only at the pore tips and the growth of pores is prohibited except for in the vertical direction (Fig. 2d). This description well explains the present results on the formation of the porous structures having a top randomly oriented pore region and a vertically oriented pore region underneath.

On the basis of this description, we assume that the average width of pore wall W_{pw} should be less than twice the width of SCR W_{SCR}, namely $W_{pw} < 2W_{SCR}$, when the vertically oriented pores start to grow. The W_{SCR} formed at the electrolyte/GaN interface is represented by

$$W_{SCR} = \left| \frac{2\varepsilon_{GaN}\varepsilon_0}{qN_D} \left(V_{EC} - V_{FB} - \frac{kT}{q} \right) \right|^{1/2}, \qquad [1]$$

where ε_0 is permittivity of vacuum, ε_{GaN} is dielectric constant of GaN, k is Boltzmann constant, T is absolute temperature, and q is elementary charge. The V_{FB} is flatband potential that was -0.9 V experimentally obtained from a Mott-Schottky plot. We obtained W_{SCR} of 100.5 nm with $V_{EC} = 10$ V from Eq. 1, and the W_{pw} is roughly estimated at 80 nm from SEM observation on the vertically oriented porous region.

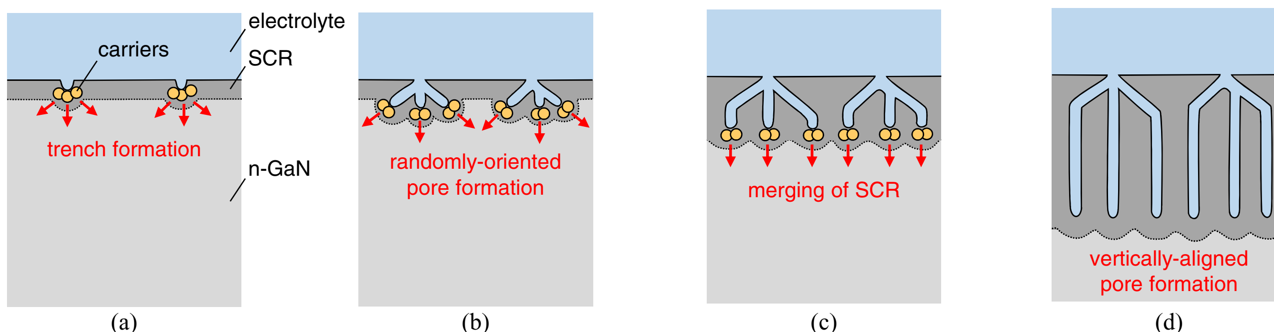

Figure 2. Schematic representations of formation flow of porous structures by anisotropic EC etching. (a) Trenches are formed and induce electric field enhancement. (b) Randomly oriented pores are formed by free carriers generated by avalanche effect. (c) The SCRs of neighboring pores merge, restricting free carrier excitation except for underneath the pore tips. (d) Pores are formed anisotropically in the vertical direction.

Downloaded on 2017-06-27 to IP 133.87.166.83 address. Redistribution subject to ECS terms of use (see ecsdl.org/site/terms_use) unless CC License in place (see abstract).

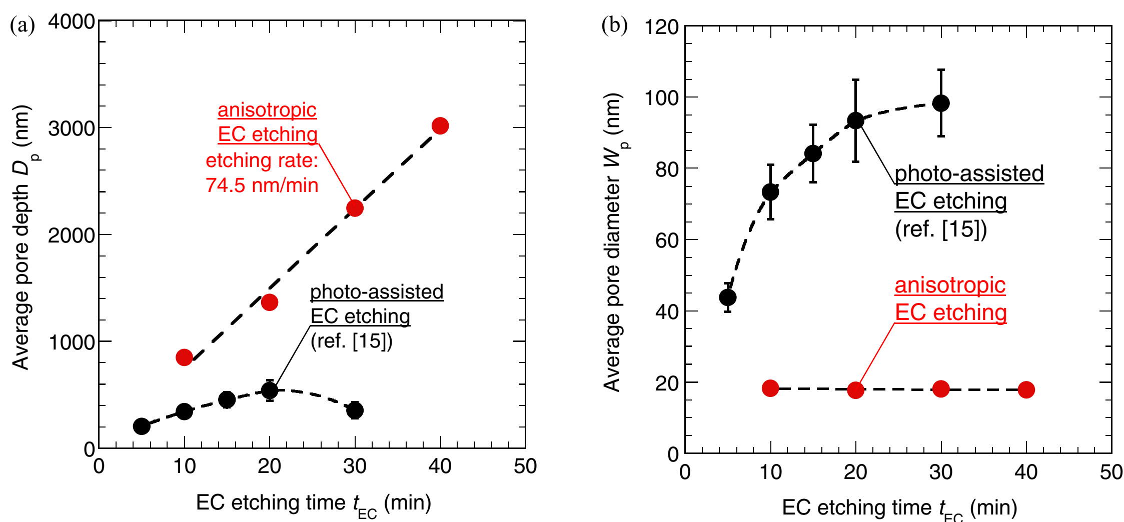

Figure 3. Average pore (a) depth D_p and (b) diameter W_p of GaN porous structures formed by photo-assisted EC etching[15] and anisotropic EC etching plotted as a function of etching time t_{EC}.

Here, one might think that the actual W_{pw} of 80 nm is too small if the lateral etching is stopped by merging the neighbor SCRs, as described in Fig. 2c. One reason for this is because the electric field concentrates preferentially at pore tips rather than pore walls under the high V_{EC} applied during the porosification. In such situation, the actual SCR of the pore wall is far thinner than the values expected by 1D calculation using Eq. 1.

Figures 3a and 3b summarizes the t_{EC}-dependence of average pore depth D_p and average pore diameter W_p, where black circles represent the results of photo-assisted EC etching obtained in our previous work[15] and red circles represent the results of anisotropic EC etching. In the case of the photo-assisted EC etching, the photo-carriers are generated on the light-irradiated surface (top surface). Since the photoelectrochemical etching occurred from the top surface along with the EC etching at the pore tips, the pore depth saturated or decreased as the etching time t_{EC} increased. On the other hand, we found that anisotropic EC etching can form deeper pores that cannot be formed by photo-assisted EC etching. We obtained deepest pores with D_p of 35.3 μm having the incredible aspect ratio of 2000 or more, which is the highest value of a GaN nanostructure to the best of our knowledge. In addition, D_p of pores formed by anisotropic EC etching has linear relationship with t_{EC}, indicating superior depth control can be achieved. This is because holes causing the etching reaction are only supplied at the pore tips as described above, where is no excess hole on the top surface. On the other hand, W_p could not be controlled with t_{EC}, as shown in Fig. 3b. This is because the width of the pore wall kept a constant value throughout the present EC etching due to its anisotropic nature.

Post wet etching of GaN porous structures using TMAH.—To explore the possibility of diameter control, we conducted wet chemical etching utilizing TMAH as subsequent treatment after the EC etching. Figures 4a and 4b shows top and cross-sectional SEM images of GaN porous structures formed by anisotropic EC etching without and with TMAH etching for 60 min. In order to evaluate structural properties accurately, randomly oriented pore regions were removed from the sample surface by reactive ion beam etching. By applying TMAH etching, pore shape changed from a round to a hexagonal shape surrounded with 6 facets of $\{1-100\}$. Average pore diameter W_p increased from 18 nm to 34 nm, but average pore depth D_p remained unchanged after the TMAH treatment. These results indicate that TMAH etching proceeds anisotropically in the horizontal direction, but not in the vertical direction of the substrate.

Generally, anisotropy in wet chemical etching is attributed to difference of etching rate; in other words, a crystallographic face with the minimum etching rate would appear. From this point of view, etching rate of the (0001) plane was almost zero, and etching rate of the $\{1-100\}$ plane was smaller than those of the other planes except for the (0001) plane. Similar results are reported by a number of previous studies on wet chemical etching of GaN using alkaline solution.[25–28] Etching-rate difference on crystallographic face is qualitatively explained by the difference of dangling bond density (DBD), which is a function of surface energy.[25,26] The DBDs of the (0001) and $\{1-100\}$ planes are 11.4 and 12.1 nm^{-2}, respectively, which is smaller than those of the other planes (e.g., $\{11-20\}$ plane (14.0 nm^{-2}) and $\{1-101\}$ plane (16.0 nm^{-2})), indicating that these planes are relatively stable toward wet chemical etching. In addition, surface polarity is also associated with etching selectivity.[27,28] On the Ga-polar (0001) plane, used in this study, three occupied dangling bonds of nitrogen appear after the 1st gallium layer is removed by the attack of hydroxide ions in the alkaline solution. Hydroxide ions cannot attack the 2nd nitrogen layer after that because of the large coulomb repul-

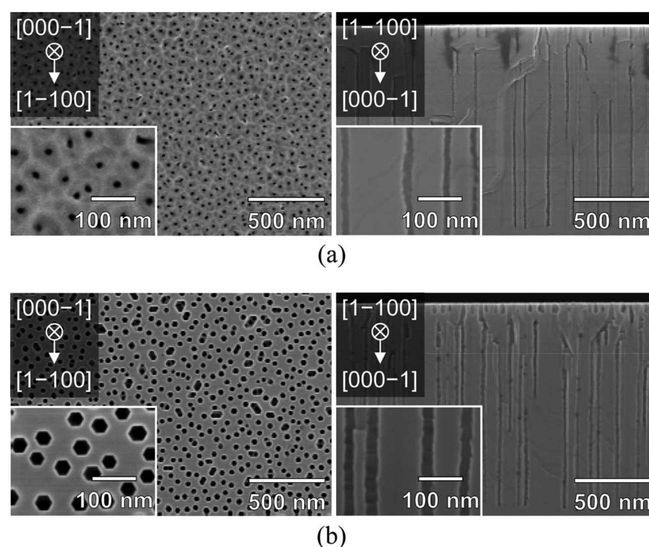

Figure 4. Top and cross-sectional SEM images of GaN porous structures formed by anisotropic EC etching (a) without TMAH etching and (b) with TMAH etching for 60 min.

Downloaded on 2017-06-27 to IP 133.87.166.83 address. Redistribution subject to ECS terms of use (see ecsdl.org/site/terms_use) unless CC License in place (see abstract).

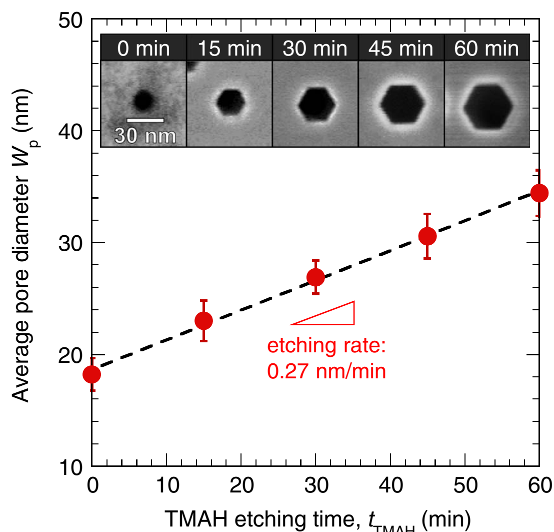

Figure 5. Relationship between average pore diameter W_p and TMAH etching time t_{TMAH}. Insets shows top SEM images of pores with different t_{TMAH}.

sion between hydroxide ions and negatively charged dangling bonds. Such self-stopping behavior would not appear on N-polar and non-polar surfaces. We believe both etching mechanisms related to DBD and surface polarity are involved, and hexagonal pores surrounded with facets of {1−100} can be obtained by TMAH etching.

Figure 5 shows the average pore diameter W_p plotted as a function of TMAH etching time t_{TMAH}, and insets show top SEM images of pores with different t_{TMAH}. There is a linear relationship between W_p and t_{TMAH} with the slow etching rate of 0.27 nm/min. Hence, post wet etching using TMAH enables us to control pore diameter precisely as well as independently from pore depth because of its anisotropic nature.

Optical and photoelectrochemical properties of GaN porous structures.—In order to gain deeper clarity about the superiority of the present GaN porous structures, optical and photoelectrochemical measurements were conducted. Figure 6a shows normalized PL spectra in the UV region obtained at room temperature from non-porous GaN and porous GaN without and with TMAH etching for 60 min. Although all samples exhibited strong near-band-edge (NBE) emission around 3.4 eV, emission peaks of two porous samples shifted toward higher energies—so-called "blue shift". The amounts of blueshift were 5.9 meV and 13.9 meV for the sample just after the anisotropic EC etching and for the sample with subsequent TMAH etching, respectively. Observation of blueshift by formation of porous structures is completely different from a number of studies on porous GaN, where the emission peaks shifted toward lower energies—so-called "red shift".[12,14] In the literature, it has been reported that redshift of NBE originates from a strain-relaxation effect, which could be caused by forming nanostructures on hetero-epitaxial GaN layers having high residual stress. In contrast, the freestanding GaN substrates used in this study were prepared by a substrate separation process that reduced substrate-induced strain,[29] where the strain-relaxation effect after the porous formation could be negligible. One possible phenomenon to explain the observed blueshift is the quantum confinement in pore walls, similar to the case of porous Si,[30] InP,[31] and our previous reports on porous GaN.[15] After the formation of porous structures, carriers were confined in two dimensions in thinned pore-walls, forming higher quantized-energy levels than the bandgap energy level. Further discussion on the basis of the systematic investigation is necessary to clarify near-band-edge emission observed from the present GaN porous structures.

Figure 6b shows the PL spectra obtained in the region from 1.8 eV to 2.6 eV, which are smaller than the bandgap of GaN. Yellow luminescence (YL) was clearly observed around 2.2 eV on the non-porous GaN. The origin of YL has been intensively discussed for a long time from both the experimental and theoretical points of view, and the accepted stance is that it is likely caused by Ga vacancy V_{Ga} and its complex with O or C.[32–34] Application of dry etching often leads to an increase of YL indicating the formation of high-density point defects. As shown in Fig. 6b, YL intensity was decreased by the formation of porous structures, suggesting that V_{Ga}-related defects were preferentially removed by EC etching. In addition, TMAH etching barely affected intensity of the YL peak. These results indicate that anisotropic EC and TMAH etching can process GaN without any damage induced.

Figure 7a shows specular reflectance spectra of a non-porous and porous GaN with different t_{TMAH}. Reflectance spectra of all porous samples were lower than those of the non-porous sample, as expected. In addition, reflectance oscillations were observed only on porous samples in the visible and near infrared regions. Local peak positions and period were changed with t_{TMAH}, indicating that oscillations were originated from optical interference between reflected light of the air/porous layer interface and that of the porous layer/substrate interface.

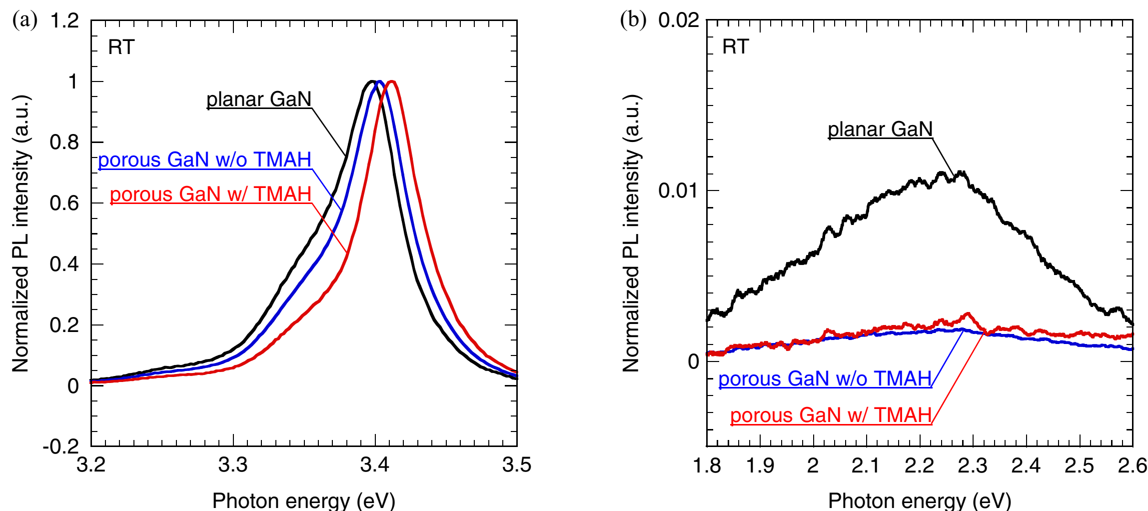

Figure 6. Normalized photoluminescence spectra of (a) UV region and (b) visible region obtained at room temperature. Black line represents planar GaN, blue line represents porous GaN without TMAH etching, and red line represents porous GaN with TMAH etching for 60 min.

Downloaded on 2017-06-27 to IP 133.87.166.83 address. Redistribution subject to ECS terms of use (see ecsdl.org/site/terms_use) unless CC License in place (see abstract).

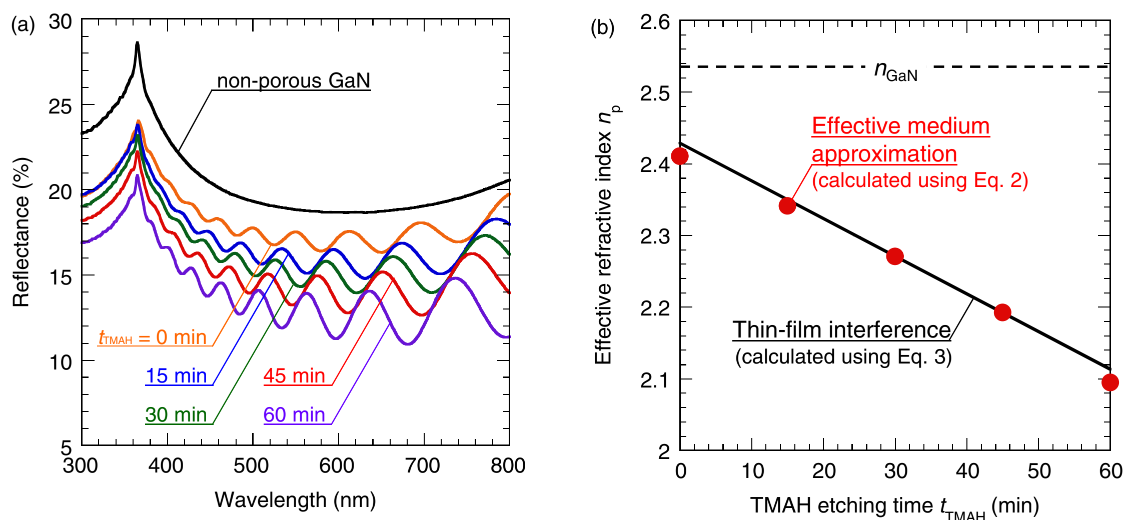

Figure 7. (a) Specular reflectance spectra of planar (black line) and porous GaN (colored line) with different TMAH etching time t_{TMAH}. (b) The t_{TMAH} dependency of effective refractive index of porous GaN calculated in accordance with effective medium approximation model (red dots) and thin-film interference model (black line).

Referring to the effective medium approximation (EMA) model, we assumed the porous layer as an air-composite material that had an effective refractive index n_p calculated by the deformed Bruggeman equation as follows:

$$f_{GaN}\frac{n_{GaN}^2 - n_p^2}{n_{GaN}^2 + n_p^2} + (1 - f_{GaN})\frac{n_{air}^2 - n_p^2}{n_{air}^2 + n_p^2} = 0, \quad [2]$$

where n_{air} and n_{GaN} are refractive index of air and GaN and f_{GaN} is volume fraction of GaN in the porous layer. In the case of the porous structures formed in this study, the f_{GaN} can easily be estimated from SEM images because the pores with a constant diameter were formed straightly in the vertical direction. In addition to the Bruggeman approach, we tried to estimate n_p with a thin-film interference model from reflectance properties. In this configuration ($n_{air} < n_p < n_{GaN}$), constructive interference occurred when the difference of optical path length corresponded with integral multiple of wavelength as follows:

$$2n_p D_p = m\lambda_{lmax}, \quad [3]$$

where m is an integer and λ_{lmax} is specific wavelength of local maximum.

The n_p values calculated from the structural properties using Eq. 2 (red circles) and reflectance properties using Eq. 3 (black solid line) are plotted in Fig. 7b as a function of TMAH etching time. Application of these models seems to be valid and feasible because the red circles and the black solid line are consistent. This agreement supports the assumption such as (1) the present porous layer is considered as an optically-homogeneous layer under the visible light and (2) the refractive index is determined by the volume fraction of nanometer-sized pores and walls. Both models indicated n_p decreased approximately linearly with t_{TMAH} whose change rate of 5.2×10^{-3} min^{-1} was very slow. From these results, superior structural controllability of anisotropic EC and TMAH etching enable us to obtain a surface with a desirable refractive index.

Finally, we evaluated the capability of our GaN porous structures as EC energy conversion systems. Figure 8a shows the current-voltage (*I-V*) characteristics of various GaN electrodes measured in 0.1 mol/L PBS under irradiation of monochromatic light ($\lambda = 350$ nm, $P_{IN} = 0.1$ mW/cm^2). For the *I-V* curves measured in the dark, all samples

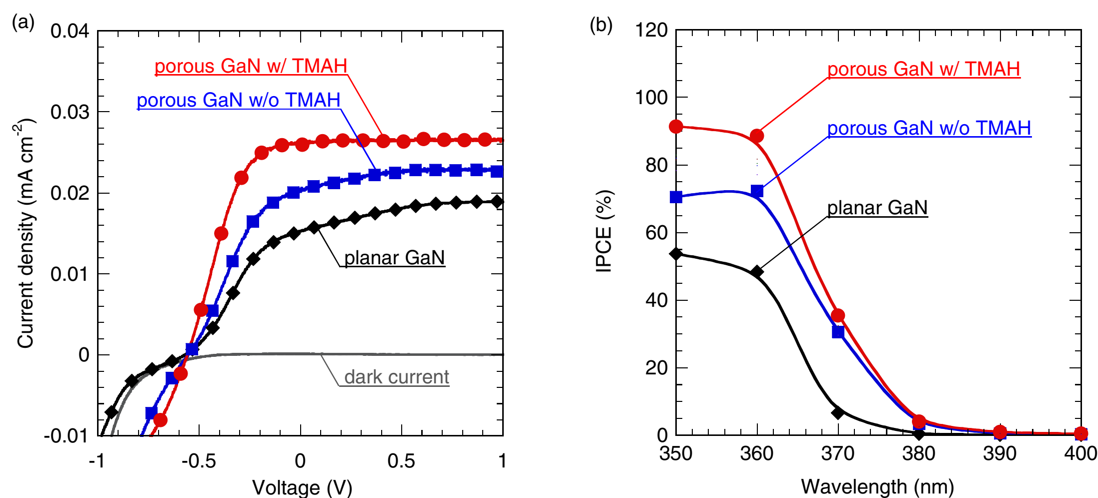

Figure 8. (a) Current-voltage characteristics under irradiation of monochromatic light ($\lambda = 350$ nm, $P_{IN} = 0.1$ mW/cm^2) and (b) IPCE at 0 V plotted as a function of wavelength. Black line represents planar GaN, blue line represents porous GaN without TMAH etching, and red line represents porous GaN with TMAH etching for 45 min.

Downloaded on 2017-06-27 to IP 133.87.166.83 address. Redistribution subject to ECS terms of use (see ecsdl.org/site/terms_use) unless CC License in place (see abstract).

showed rectifying properties similar to the case of Schottky barrier diodes. Here, negative currents were observed at negative bias because cathodic reactions were caused by electrons, which are majority carriers in n-GaN. On the other hand, few positive currents were observed at the entire bias range because anodic reactions were barely caused due to lack of holes, which are minority carriers in n-GaN.

Under irradiation of light, positive currents were observed as photocurrents on all samples, indicating photo-generated carriers were separated by potential gradient in SCR and contributed to EC reactions. Rest potentials, at which positive current started to flow, of all samples were almost the same value of −0.58 V, but the bias-dependent behavior of photocurrents is changed by the surface geometry of GaN. The photocurrent of non-porous GaN started to flow at around −0.5 V and kept increasing slightly until 1.0 V. This is a typical behavior observed on planar photoelectrodes, where the amount of charge carriers contributing to the photocurrents increased with the SCR width W_{SCR} as a function of the applied voltage, as described in Eq. 1.[1] On the other hand, the photocurrents of porous GaNs saturated at specific voltage, showing less dependent-change with the applied voltage. In porous samples, charge carriers would be generated in the porous region, not in the bulk region underneath, because light penetration depth is much shorter than pore depth. Therefore, the charge carriers can easily reach the SCR formed in the pore walls even though the pore wall is not completely depleted and W_{SCR} is small at low bias such as 0 V. In such situation, the charge carriers generated in the pore walls can be immediately separated, leading to the steep increase of photocurrents up to the saturation value. This phenomenon of "efficient carrier separation" is one of the attractive features and big advantages of porous structures for EC energy conversion systems because the highest photocurrent can be obtained even at a lower bias such as 0 V. In addition, we found that photocurrent-saturated bias shifted from 0.6 V to −0.1 V by subsequent TMAH etching. This was because the increase of pore diameter W_p enhanced "efficient carrier separation" due to the increase of the ratio of W_{SCR} to the pore wall width W_{pw}.

Figure 8b shows the incident-photon-to-current conversion efficiency (IPCE) measured at 0 V as a function of light wavelength λ. IPCE of 54% at 350 nm was obtained on non-porous GaN, which is almost the same value as a previous report.[35] Compared to that, IPCE was enhanced by the formation of porous structures to as high as 70%, and enhanced furthermore by subsequent TMAH etching to as high as 91%. These results clearly demonstrate that the formation of porous structures is effective for yielding high IPCE in EC energy conversion systems due to their attractive features mentioned above. It is also noted that photocurrent under the light with photon energy below the GaN bandgap was dramatically improved by the formation of porous structures. We believe this is due to enhancement of Franz-Keldysh effect: namely, the high electric field induced at pore tips causes redshift of the photoabsorption edge.[16,36,37]

We further investigated the effect of TMAH etching time t_{TMAH} on IPCE. As shown in Fig. 9a, IPCE increased from 70% to 91% with t_{TMAH} up until 45 min, but it decreased with $t_{TMAH} = 60$ min, although the structural change was only several nanometers. In order to explain the IPCE behavior toward t_{TMAH}, we assumed that the separation- and correction-efficiency of the photo-carriers generated in the pore walls is strongly affected by the width of pore wall W_{pw}. Figures 9b and 9c shows the width of quasi-neutral region W_{QNR} and flatband potential V_{FB}, respectively, whose definition and relation are schematically described in Fig. 9d. If the W_{pw} is more than twice the size of the W_{SCR}, the pore wall consists of SCRs and the quasi-neutral region illustrated in the left diagram of Fig. 9d. Here, W_{QNR} and V_{FB} can be represented as

$$W_{QNR} = W_{pw} - 2W_{SCR}, \quad [4]$$

$$|V_{FB}| = \frac{qN_D}{2\varepsilon_{GaN}\varepsilon_0} W_{SCR}^2. \quad [5]$$

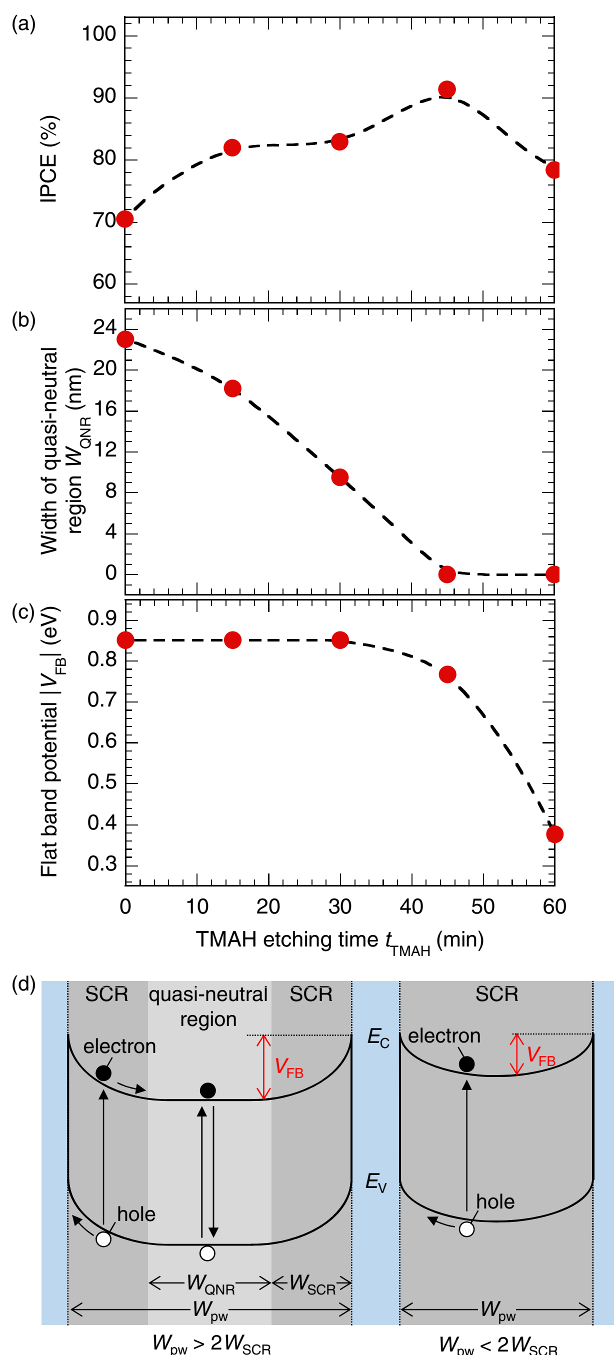

Figure 9. The t_{TMAH} dependency of (a) IPCE at 0 V, (b) width of quasi-neutral region W_{QNR}, and (c) modulus of flatband potential $|V_{FB}|$. (d) Schematic representations of energy band diagrams in pore wall if $W_{pw} > 2W_{SCR}$ (left) or $W_{pw} < 2W_{SCR}$ (right).

If the W_{pw} is less than twice the size of the W_{SCR}, the pore wall is fully depleted and the quasi-neutral region disappears, as illustrated in the right diagram of Fig. 9d. In such situation, W_{QNR} will be zero and V_{FB} can be obtained by the following approximation:

$$|V_{FB}| = \frac{qN_D}{2\varepsilon_{GaN}\varepsilon_0}\left(\frac{W_{pw}}{2}\right)^2. \quad [6]$$

The two kinds of plots for W_{QNR} and V_{FB}, respectively shown in Figs. 9b and 9c, were calculated using Eqs. 4–6 and W_{pw} obtained from SEM observation.

Downloaded on 2017-06-27 to IP 133.87.166.83 address. Redistribution subject to ECS terms of use (see ecsdl.org/site/terms_use) unless CC License in place (see abstract).

As shown in Fig. 9b, W_{QNR} decreased with t_{TMAH} in a reflection to the W_{pw} changed by the TMAH treatment, where W_{QNR} becomes zero with $t_{TMAH} \geq 45$ min. The V_{FB} was changed closely in the relation between W_{QNR} and W_{pw} as shown in Fig. 9c. Namely, the V_{FB} started to decrease at around $t_{TMAH} = 45$ min when the pore walls were fully depleted and the W_{QNR} disappeared. The V_{FB} further decreased to 0.4 eV with $t_{TMAH} = 60$ min, whose value is almost half of the initial value obtained with $t_{TMAH} = 0$ min.

The semi-qualitative analysis above indicates that the highest IPCE value was obtained when the W_{QNR} is just on zero at around $t_{TMAH} = 45$ min. The contribution of the photo-carriers for the photocurrents becomes larger as the W_{QNR} decreases, because "efficient carrier separation" was enhanced. On the other hand, the ability of the carrier-separation becomes smaller as the V_{FB} decreases, because the electric field in the SCR decreases. Lower V_{FB} also led to photocurrent reduction by recombination in SCR region, as predicted by Sah et al.[38] From the above discussion, one possible reason the highest IPCE could be obtained with $t_{TMAH} = 45$ min is that recombination is suppressed because W_{pw} is almost the same with twice the W_{SCR}. We conclude that precise structural controlling is crucially important to obtain superior capability for EC energy conversion systems, and the two-step process utilizing anisotropic EC etching and TMAH etching is very promising as a nanostructure fabrication technique.

Conclusions

We have developed EC etching and TMAH wet etching to fabricate GaN porous structures with improved structural controllability. Superior controllability in depth and diameter could be obtained by achieving anisotropic nature in the direction of [000−1] by EC etching and [1−100] by TMAH etching. We could control pores in the wide range between sub-μm to tens of μm in depth and 18 to 50 nm in diameter. From PL measurements, porous samples showed blueshift of NBE emission due to quantum confinement in the pore wall. Reduction of YL intensity was also observed, indicating V_{Ga}-related defects were preferentially removed and additional damage was not induced by this method. Photoreflectance measurement revealed that porous samples had an effective refractive index that could be controlled by TMAH etching time. In photoelectrochemical measurement, IPCE was dramatically enhanced to as high as 91% by the formation of porous structures with adequate structural properties. These results clearly show that the precisely controlled GaN porous structure by two-step anisotropic etching is very promising as an electrode in EC energy conversion systems.

Acknowledgments

This work was supported in part by a Grant-in-Aid for JSPS Fellows 14J01371 and by JSPS KAKENHI grant Numbers JP15K13937 and JP16H06421.

References

1. I. M. Huygens, K. Strubbe, and W. P. Gomes, *Journal of the Electrochemical Society*, **147**, 1797 (2000).
2. J. D. Beach, R. T. Collins, and J. A. Turner, *Journal of the Electrochemical Society*, **150**, A899 (2003).
3. K. Fujii, T. K. Karasawa, and K. Ohkawa, *Japanese Journal of Applied Physics*, **44**, L543 (2005).
4. S. Yotsuhashi, M. Deguchi, Y. Zenitani, R. Hinogami, H. Hashiba, Y. Yamada, and K. Ohkawa, *Applied Physics Express*, **4**, 117101 (2011).
5. T. Sato, N. Yoshizawa, and T. Hashizume, *Thin Solid Films*, **518**, 4399 (2010).
6. Y. Kumazaki, T. Kudo, Z. Yatabe, and T. Sato, *Applied Surface Science*, **279**, 116 (2013).
7. Y. D. Wang, K. Y. Zang, and S. J. Chua, *Journal of Applied Physics*, **100**, 054306 (2006).
8. I. Waki, D. Cohen, R. Lal, U. Mishra, S. P. DenBaars, and S. Nakamura, *Applied Physics Letters*, **91**, 093519 (2007).
9. H. Ono, Y. Ono, K. Kasahara, J. Mizuno, and S. Shoji, *Japanese Journal of Applied Physics*, **47**, 933 (2008).
10. W. M. Zhou, G. Q. Min, Z. T. Song, J. Zhang, Y. B. Liu, and J. P. Zhang, *Nanotechnology*, **21**, 405304 (2010).
11. A. P. Vajpeyi, S. J. Chua, S. Tripathy, and E. A. Fitzgerald, *Applied Physics Letters*, **91**, 083110 (2007).
12. H. Hartono, C. B. Soh, S. J. Chua, and E. A. Fitzgerald, *Journal of the Electrochemical Society*, **154**, H1004 (2007).
13. K. Al-Heuseen, M. R. Hashim, and N. K. Ali, *Journal of the Electrochemical Society*, **158**, D240 (2011).
14. K. P. Beh, F. K. Yam, L. K. Tan, S. W. Ng, C. W. Chin, and Z. Hassan, *Japanese Journal of Applied Physics*, **52**, 08JK03 (2013).
15. Y. Kumazaki, A. Watanabe, Z. Yatabe, and T. Sato, *Journal of the Electrochemical Society*, **161**, H705 (2014).
16. Y. Kumazaki, Z. Yatabe, and T. Sato, *Japanese Journal of Applied Physics*, **55**, 04EJ12 (2016).
17. M. Kodama, M. Sugimoto, E. Hayashi, N. Soejima, O. Ishiguro, M. Kanechika, K. Itoh, H. Ueda, T. Uesugi, and T. Kachi, *Applied Physics Express*, **1**, 021104 (2008).
18. K.-W. Kim, S.-D. Jung, D.-S. Kim, H.-S. Kang, K.-S. Im, J.-J. Oh, J.-B. Ha, J.-K. Shin, and J.-H. Lee, *IEEE Electron Device Letters*, **32**, 1376 (2011).
19. J. F. Muth, J. H. Lee, I. K. Shmagin, R. M. Kolbas, H. C. Casey, Jr. B. P. Keller, U. K. Mishra, and S. P. DenBaars, *Applied Physics Letters*, **71**, 2572 (1997).
20. C. Youtsey, L. T. Romano, and I. Adesida, *Applied Physics Letters*, **73**, 797 (1998).
21. C. B. Soh, C. B. Tay, R. J. N. Tan, A. P. Vajpeyi, I. P. Seetoh, K. K. Ansah-Antwi, and S. J. Chua, *Journal of Physics D: Applied Physics*, **46**, 365102 (2013).
22. M. I. J. Beale, N. G. Chew, M. J. Uren, A. G. Cullis, and J. D. Benjamin, *Applied Physics Letters*, **46**, 86 (1985).
23. V. Lehmann and H. Foll, *Journal of the Electrochemical Society*, **137**, 653 (1990).
24. L. Santinacci, A.-M. Goncalves, N. Simon, and A. Etcheberry, *Electrochimica Acta*, **56**, 878 (2010).
25. J. Liu, J. Huang, X. Gong, J. Wang, K. Xu, Y. Qiu, D. Cai, T. Zhou, G. Ren, and H. Yang, *CrystEngComm*, **13**, 5929 (2011).
26. W. Chen, J. Lin, G. Hu, X. Han, M. Liu, Y. Yang, Z. Wu, Y. Liu, and B. Zhang, *Journal of Crystal Growth*, **426**, 168 (2015).
27. D. Li, M. Sumiya, S. Fuke, D. Yang, D. Que, Y. Suzuki, and Y. Fukuda, *Journal of Applied Physics*, **90**, 4219 (2001).
28. M. Itoh, T. Kinoshita, C. Koike, M. Takeuchi, K. Kawasaki, and Y. Aoyagi, *Japanese Journal of Applied Physics*, **45**, 3988 (2006).
29. V. Darakchieva, T. Paskova, P. P. Paskov, B. Monemar, N. Ashkenov, and M. Schubert, *Physica Status Solidi*, **195**, 516 (2003).
30. L. T. Canham, *Applied Physics Letters*, **57**, 1046 (1990).
31. T. Fujino, T. Sato, and T. Hashizume, *Japanese Journal of Applied Physics*, **46**, 4375 (2007).
32. T. Ogino and M. Aoki, *Japanese Journal of Applied Physics*, **19**, 2395 (1980).
33. J. Neugebauer and C. G. Van de Walle, *Applied Physics Letters*, **69**, 503 (1996).
34. M. A. Reshchikov and H. Morkoç, *Journal of Applied Physics*, **97**, 061301 (2005).
35. T. Hayashi, M. Deura, and K. Ohkawa, *Japanese Journal of Applied Physics*, **51**, 112601 (2012).
36. A. Watanabe, Y. Kumazaki, Z. Yatabe, and T. Sato, *ECS Electrochemistry Letters*, **4**, H11 (2015).
37. T. Sato, Y. Kumazaki, H. Kida, A. Watanabe, Z. Yatabe, and S. Matsuda, *Semiconductor Science and Technology*, **31**, 014012 (2016).
38. C.-T. Sah, R. N. Noyce, and W. Shockley, *Proceedings of the IRE*, **45**, 1228 (1957).

Downloaded on 2017-06-27 to IP 133.87.166.83 address. Redistribution subject to ECS terms of use (see ecsdl.org/site/terms_use) unless CC License in place (see abstract).